ST-ECF Instrument Science Report ACS 2005-002

Flat-field and sensitivity calibration for ACS G800L slitless spectroscopy modes

J. R. Walsh, N. Pirzkal
February 24 2005

ABSTRACT

Flat-fields are an essential component in creating scientific quality images of uniform sensitivity. For filter imaging, a single flat-field or a combination of a low spatial frequency and a pixel-to-pixel flat suffices. However for slitless spectroscopy data, a flat-field must effectively be provided at each wavelength of the spectral sensitivity, since each pixel can receive any wavelength. The flat-fielding of the ACS WFC and HRC for the G800L grism is described. For slitless spectroscopy data the flat-field can be described as a cube with the spatial dimensions those of the detector and the 3rd dimension that of wavelength. Two options are available for forming the ACS flat-field cube: to use the ground-based flat-fields taken with a monochromator or to use the in-orbit filter flats. On account of the vignetting problems affecting the ground-based flats, in-orbit flats have been used. The contruction of this flat-field is described.

The efficacy of this flat-field cube has been investigated from observations of a spectrophotometric standard at different positions in the field. By requiring the extracted spectra from different positions over the field to match in flux, a smooth function was derived and applied to the flat-field cube. The single sensitivity curve for the whole detector area is then determined from the mean spectrum at the different positions. Good results are reported with rms deviations in the shape of extracted spectra <2% across the WFC field and about 1% in the HRC, except at the blue and red edges of the wavelength range. These flat-fields and sensitivity curves are supplied for routine spectral extraction of ACS slitless spectral data as part of the aXe package.

1. Introduction

In the ACS, the off-axis nature of the instrument and the many optical elements result in a raw image of a uniformely bright region of the sky, devoid of sources, being far from flat. The largest effect for the ACS is the geometric distortion of the optics but, for a given filter, effects such as vignetting and varying wavelength response of the detector across its area also contribute. In the presence of geometric distortion, a uniform sky brightness is not detected as a constant signal per pixel at the detector on account of the varying pixel size over the field. The usual method to remove the instrument and detector signature for a given filter is a filter flat-field. Application of the flat-field, which in the case of HST instruments is usually decomposed into two parts - a low spatial frequency part (L-flat) and a high spatial frequency or pixel flat (P-flat) - should then result in flat sky images. In the case of ACS, the correction by the L-flat-field produces a flat image for an input flat sky. The surface intensity of a point is correct in the flat-fielded image, but photometry of the total flux of an object is not, on account of the varying pixel area projected on the sky. The “drizzle” task in STSDAS (Fruchter & Hook, 2002), which maps surface intensity, removes the geometric distortion by converting all pixels to the same projected size on the sky. This results in an image in which both surface and total object photometry are correct. In the case of filter imaging data, one flat-field correction (a combination of the L- and P-flats) suffices for the complete correction. However, for slitless spectroscopy data, each pixel can receive radiation of any wavelength allowed by the disperser and thus each pixel must be corrected over this wavelength range. It follows that a series of flat-fields over the passband of the disperser is required. This leads to the implementation of a flat-field cube (two spatial dimensions and one wavelength) which is capable of providing a flat-field at every wavelength over the disperser range.

This ISR describes the construction of flat-fields for the ACS G800L grism for both the Wide Field and High Resolution Channels (WFC and HRC respectively). Some ground-based images were obtained with a monochromator with the aim of providing flat-field data. With ACS in orbit it is not possible to obtain monochromatic wavelength dependent flat-field data for the grism and so resort was made to the filter flat-fields. The construction of the flat-fields from the filter LP flats is decribed. Slitless spectra of spectrophotometric stars at different positions over the field enabled the efficacy of the flat-fielding procedure to be tested and thus a single sensitivity (conversion from detector to flux units) to be achieved. The flat-field cubes for the WFC and HRC are used in the aXe package (Pirzkal et al. 2002; http://www.stecf.org/software/aXe/index.html) for extraction of ACS slitless data.

2. Narrow-band ground flats

During the ground testing program at Ball Aerospace a monochromator and the Refractive Aberration Simulator / Hubble Opto-Mechanical Simulator (RAS/HOMS) was used to

obtain a series of narrow-band images at a variety of wavelengths over the G800L pass-band (5000-11000A). The primary purpose of this experiment was to measure the fringing of the ACS WFC and HRC detectors. The data and derivation of the fringing is described in Walsh et al. (2003) where a list of all the ground-based flat-field images is available. Although the wavelength coverage is sparse and incomplete (only covering 7000 to 10000A), the fact that these are monochromatic flats make them, in principle, very useful for fitting the variation of the flat-field with wavelength.

Narrow-band flat-field images were formed from the bias-subtracted monochromator images. The images were Gaussian smoothed with a large sigma (40 pixels for WFC, 35 pixels for HRC) to completely remove the effects of fringing . A simple normalization to the mean of a large area excluding a 100 pixel width at the chip edges was applied. Several 100x100 pixel areas were selected on the chips and the mean flat-field was computed for each narrow-band flat. Figure 1 shows the mean normalised flat-fields for three regions over WFC Chip 1 (Figure 1, upper) and over WFC Chip 2 (Figure 1, lower). In Figure 2 the mean flat-field values in three square regions selected over the HRC are shown. It is clear from these plots that there are very distinct colour properties of the flat-field with wavelength which varies with position over the chips. This is probably primarily attributable to the varying thickness of the Si detection layer in the back-illuminated (SITe) chips; also the different thicknesses of the layers in the multi-layer coating may also contribute (see Walsh et al. 2003). In Figures 1 and 2 low order (3rd) polynomials have been fitted by unweighted least squares to the wavelength variation of the flat-fields and appear to do a fair job at representing the wavelength dependent variation. The typical rms on the fits is 0.5-1.2% for the WFC (46 points) and around 0.7% for the HRC (37 points).

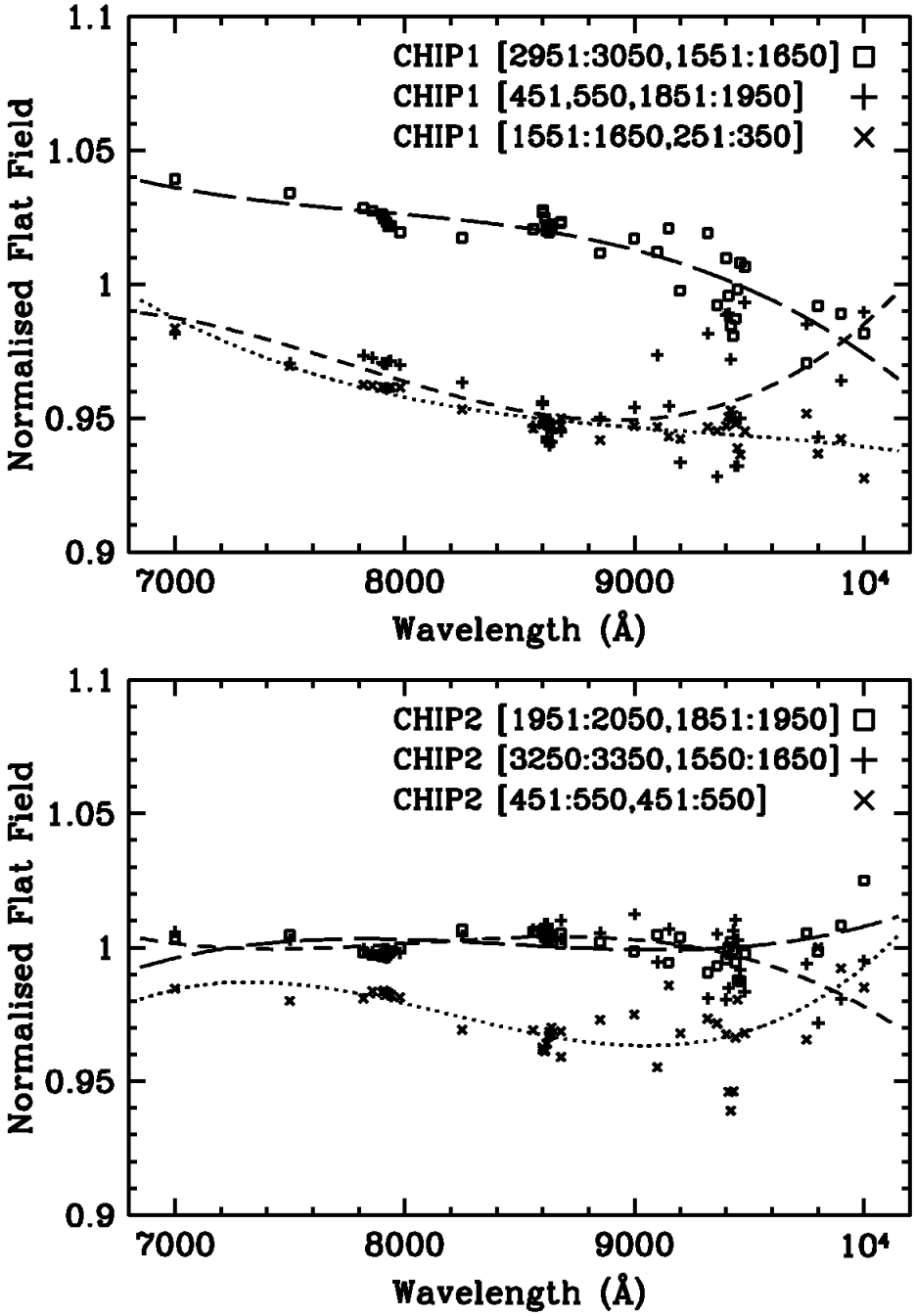

Figure 1: The normalised flat-field values, for the ground calibration data, measured in square apertures over the WFC, are plotted as a function of wavelength. The flat-field values correspond to regions which are listed in the figure for each chip (using different symbols) with Chip 1 at the top and Chip 2 below. 3rd order polynomial fits to the points are shown.

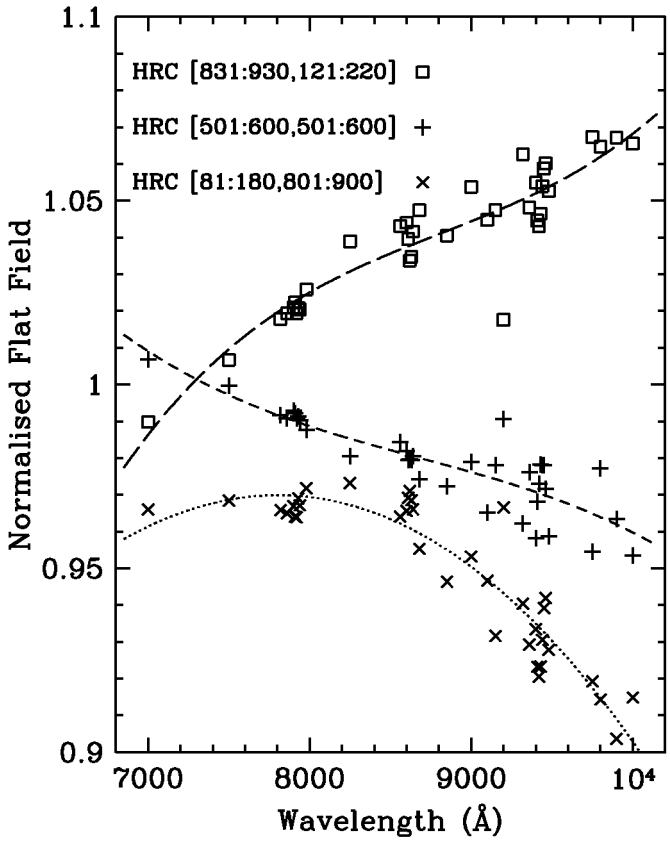

Figure 2: An identical plot to the one for the WFC chips in Figure 1 is shown for the HRC from the ground-based monochromatic flat fleld data.

3. In-orbit flats

ACS in-orbit filter L-flats were constructed using multiple dithered observations in many filters over globular clusters (Mack et al., 2002) using the method described in van der Marel (2003). For use in the ACS image reduction pipeline, combined LP flats are used: these flat-fields were constructed by dividing the ground-based pixel flat-fields by the in-orbit L-flats, as described by Mack et al., 2002. The flat field is applied before any correction for geometric distortion. These LP flat-fields provide a potentially useful set for constructing G800L wavelength dependent flats. In comparison with the ground narrow-band flats they present some advantages and disadvantages. Among the advantages are: the wavelength coverage is better to short wavelengths (no monochromatic ground flats below 7000A); the photometric accuracy has been carefully tested. Among the disadvantages are: there are rather few filters over the G800L grism range (5500-10500A); no in-orbit flat-fields are available beyond 9500A; many of the filters are broad, so only the central wavelength is used and variations in response across the filter passband remain lost.

Bohlin (2002) however showed that the variation of the LP-flat-field is smooth over the wavelength range of the G800L so use of broader filters to fit the wavelength response should be adequate. However the most telling reason why the in-orbit flats must be employed for the grism flat-field is that the ground filter flats were found not to match the in-orbit flats. Mack et al (2002) report that the ground flats cause stellar photometry differing by +/- 9% from the in-orbit flats, the latter established to provide photometric uniformity to around 1%. The cause of this is not well known but is considered to be spatial and wavelength dependent illumination of the RAS/HOMS beam into ACS. Thus despite some disadvantages, the in-orbit flats are a more reliable source for the derivation of the G800L flat-field cube.

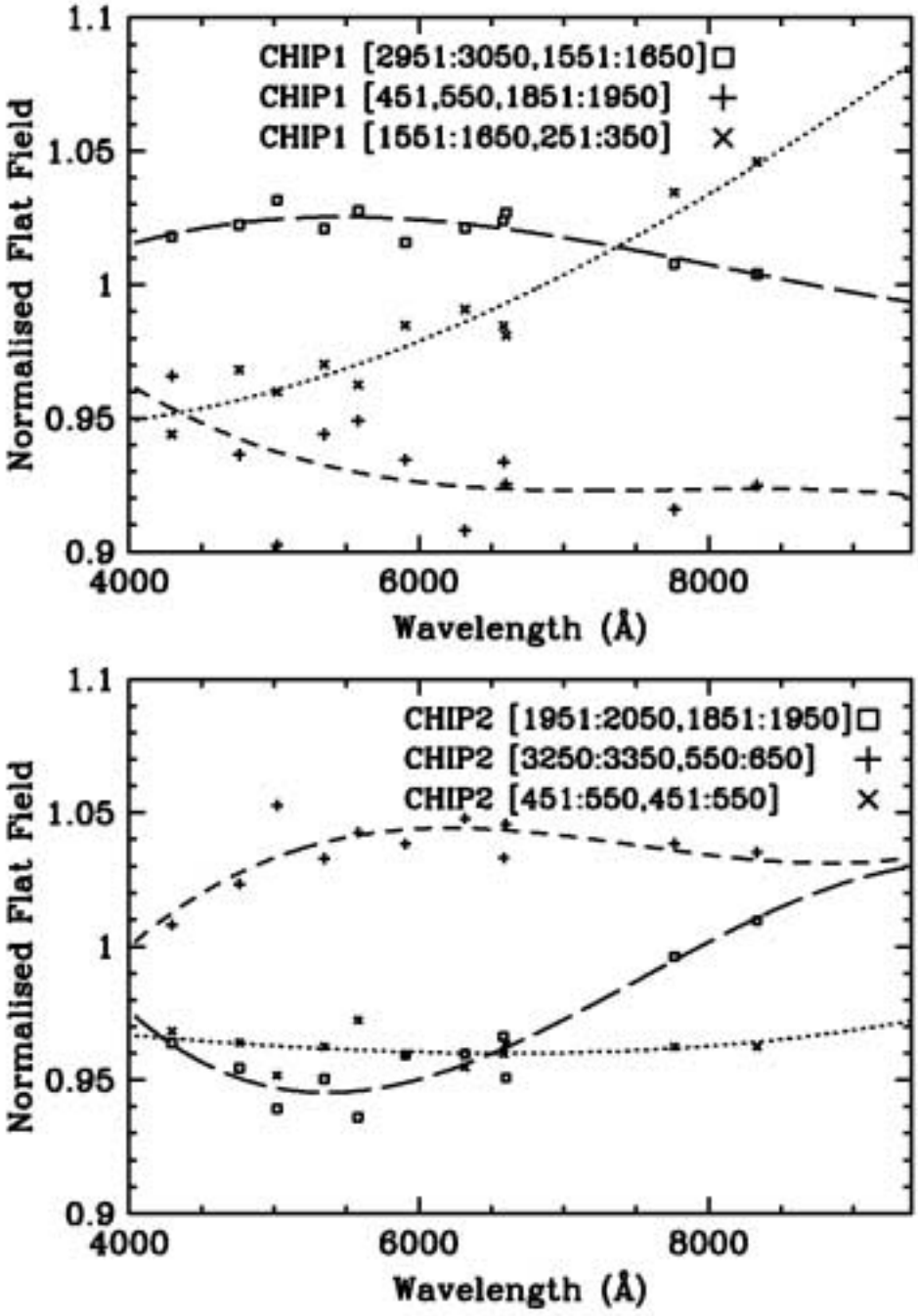

Figure 3: The mean values in square apertures for the in-orbit flat-fields with the WFC, are plotted as a function of wavelength. The flat-field values correspond to regions which are listed in the figure and 3rd order polynomial fits are shown by lines.

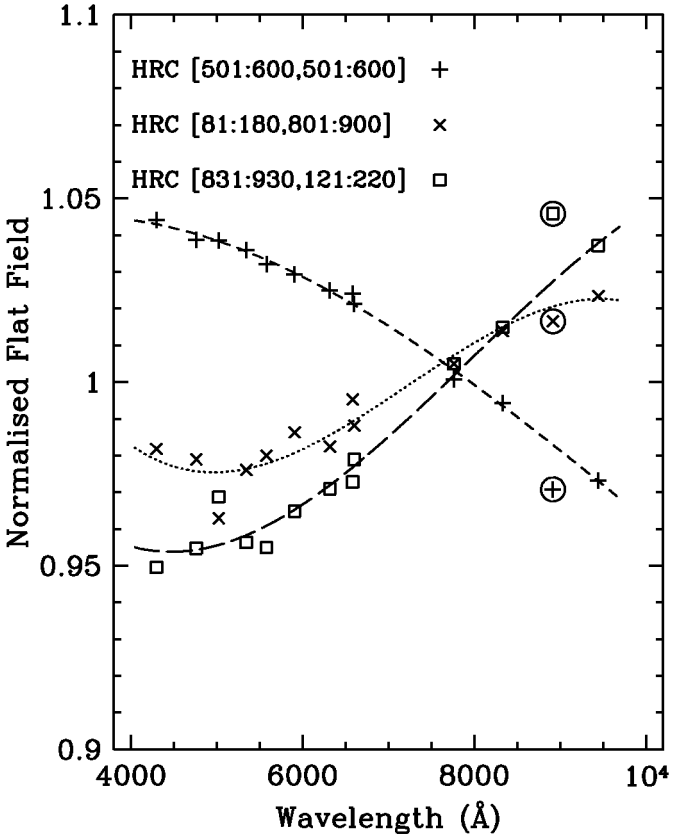

Figure 4: The mean values in square apertures of the in-orbit flat-fields for the HRC, are plotted as a function of wavelength. The flat-field values correspond to regions which are listed in the figure and 3rd order polynomial fits are shown by lines. The circled points are for the F892N filter which suffers the most from the effects of detector fringing.

In Figure 3 are plotted the in-orbit LP flat-field variation with wavelength at a number of positions on the WFC chip as a function of central wavelength of the ACS filters (values taken from the ACS Instrument Handbook, Pavlovsky et al., 2004, Tables 4.1 and 4.2). Third order polynomials are again fitted using least squares. Figure 4 shows the same plot as Figure 2 for the HRC with the in-orbit flats. The rms on the polynomials fits are <1.4%for WFC CHIP1, <0.7% for CHIP 2 (for 12 points) and <0.48% for the HRC (12 points). The F892N filter is only 150A wide and suffers the most from fringing: the points corresponding to this filter are shown circled in Figure 4, and, given their relatively large deviation from the least squares polynomial fit, were not considered in the fitting. Comparison of Figures 1 and 3 and 2 and 4 is illustrative of differences in the results of the two flat-fielding methods. The comparison is shown directly in Figure 5 where the flat-field values using the two techniques - ground-based narrow band flats (points) and in-orbit filter flats (fits as lines) - are plotted for the WFC CHIP 1 in the region of overlap. It is clear that adopting the fits from the ground flat-field data would lead to errors of many percent

when applied to in-orbit data. The exact nature of this discrepancy has not been well explianed but presumably derives from dispersive elements in the illuminating beam of the ground test setup. From these plots it is also clear that flat-fielding grism data by a single filter flat, say F775W which covers the peaks of the response, would lead to considerable errors at longer and shorter wavelengths, amounting to 5% or more in some cases, depending exactly where on the detector the spectrum lies.

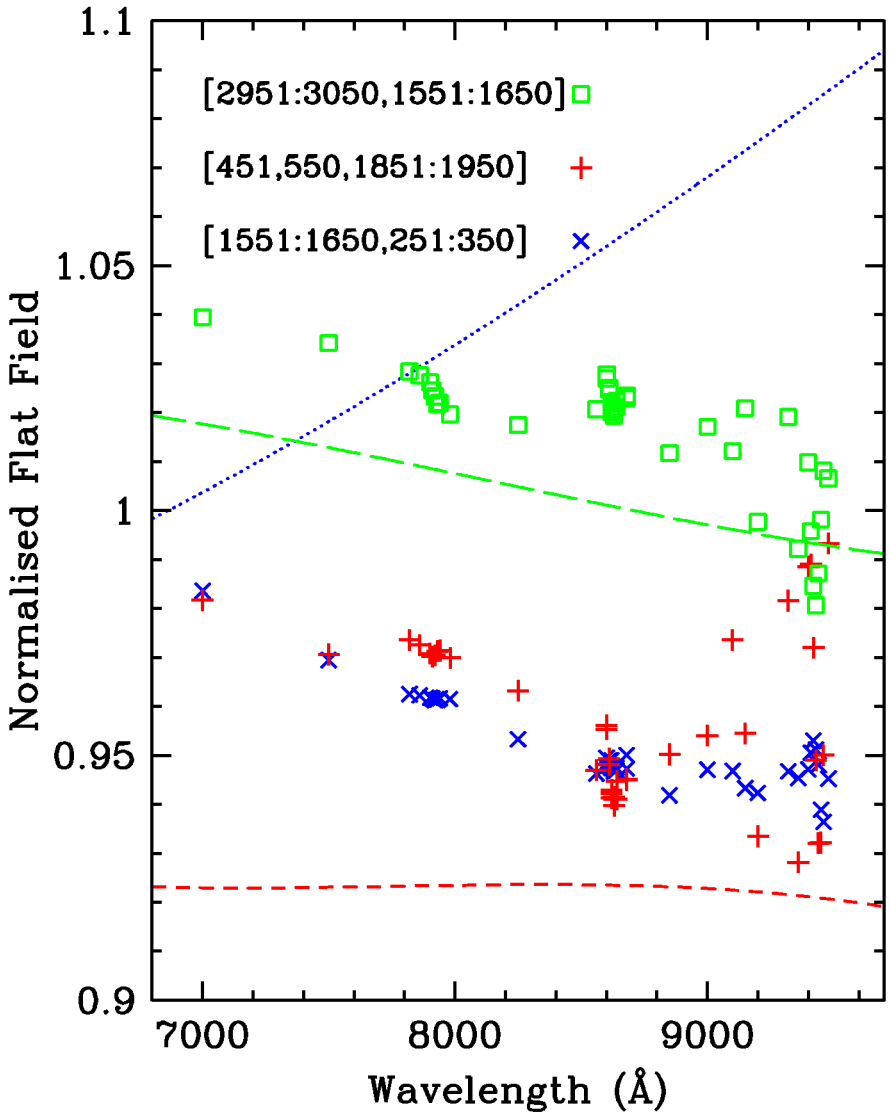

Figure 5: For WFC CHIP1 the points from the normalised ground flat-fields in the apertures listed are compared with the fits (lines) from the in-orbit flat-fields for the same areas. The points and lines are colour-coded to distinguish the values for the same aperture.

4. Production of WFC and HRC flat-field cubes

The ACS WFC and HRC in-orbit LP flat-fields were least squares fitted by a 3rd order polynomial as a function of wavelength at each pixel. The polynomial coefficients of this fit were copied to multi-association FITS images, with the [0] association as the constant term and the [1], [2] and [3] associations as the 1st, 2nd and 3rd order terms respectively. A dedicated task (flatcube) was written in IRAF/F77VOS to perform the fitting and an rms image was also produced to assess the goodness of fit.
The results of this fit allow the creation of a data cube covering any wavelength over the range of the G800L grism (5000-11000A) enabling aXe to compute and apply the proper flat-fielding correction at any pixel position and wavelength. Also required, in the FITS header of the flat fleld cube are the start and end wavelengths (keywords WMIN and WMAX respectively) since the polynomial fit must be in terms of scaled wavelength for compatibility with aXe. The flat-fielding step needs to be applied during the spectral extraction process since the wavelength extent of the light detected at a given pixel must be known before the appropriate flat-fielding correction, which is applied to both object and backgound pixels, can be computed. The wavelength range of a given pixel is calculated from the position of the direct image producing the spectrum and a configuration file defining the spectrum trace and the dispersion solution. The efficacy of the flat-field correction can be tested through slitless spectra of a standard source at different positions over the field.

5. White dwarf calibration observations

5.1 WFC

Two white dwarfs were observed using the WFC G800L grism mode: GD153 during the ACS SMOV campaign and G191B2B during the Cycle 11 Interim Calibration (proposal 9568). GD153 was observed at five different positions which were read-out using ACS subarrays (3000 x 400 pixels in X,Y). Unfortunately, the target position did not always end up at the center of the subarray and this resulted in only two useful positions where the first order spectra were completely within the subarray. The spectra at the other positions were truncated and did not contain all the flux from GD153 at each wavelength.
G191B2B, was observed using the same technique but at 10 different positions, 5 in the upper half of the detector (CHIP1) and 5 in the lower part (CHIP2). The G191B2B spectra were all completely within each aperture and most positions were observed twice for a total of 18 G800L grism exposures, and 18 companion direct images. Table 1 contains brief details of the observations. Figure 1 of Pasquali et al. (2003) shows the positions of the various pointings over the field of view of the WFC (WFC1 W0 in Table 1 corresponds to “Centre” of WFC1 in Figure 1 of Pasquali et al. 2003a). Only the WFC G191B2B data will be considered further.

Image	Pointing	Date	Filters	Exp.(s)
j8eu04aeq	WFC1 W7	2002-07-31	F775W	1
j8eu04afq			G800L	15
j8eu04agq	WFC1 W7	2002-07-31	F775W	1
j8eu04ahq			G800L	15
j8eu04ajq	WFC1 W8	2002-07-31	F775W	1
j8eu04akq			G800L	15
j8eu04amq	WFC1 W0	2002-07-31	F775W	1
j8eu04anq			G800L	15
j8eu04aoq	WFC1 W0	2002-07-31	F775W	1
j8eu04apq			G800L	15
j8eu05b5q	WFC2 W2	2002-07-31	F775W	1
j8eu05b6q			G800L	15
j8eu05b8q	WFC2 W5	2002-07-31	F775W	1
j8eu05b9q			G800L	15
j8eu05baq	WFC2 W5	2002-07-31	F775W	1
j8eu05bbq			G800L	15
j8eu05bgq	WFC2 W1	2002-07-31	F775W	1
j8eu05bhq			G800L	15
j8eu05biq	WFC2 W1	2002-07-31	F775W	1
j8eu05bjq			G800L	15
j8eua4asq	WFC1 W9	2002-07-31	F775W	1
j8eua4atq			G800L	15
j8eua4auq	WFC1 W9	2002-07-31	F775W	1
j8eua4avq			G800L	15
j8eua4azq	WFC1 W10	2002-07-31	F775W	1
j8eua4b0q			G800L	15
j8eua4b1q	WFC1 W10	2002-07-31	F775W	1
j8eua4b2q			G800L	15
j8eua5bmq	WFC2 W4	2002-07-31	F775W	1
j8eua5bnq			G800L	15
j8eua5boq	WFC2 W4	2002-07-31	F775W	1
j8eua5bpq			G800L	15
j8eua5buq	WFC2 W3	2002-07-31	F775W	1
j8eua5bvq			G800L	15
j8eua5awq	WFC2 W3	2002-07-31	F775W	1
j8eua5bxq			G800L	15

Table 1. Log of the observations of G191B2B with the ACS WFC in programme 9568.

The ACS pipeline calacs was run on the raw data files and the bias subtracted and gain corrected (_FLT) files were used in subsequent processing. The pipeline output CR cleaned files (_CRJ) could equally well have been used, but no CR-split image sets were obtained during these observations.The default ACS pipeline setting for grism data is not to flat-field. No correction for the fringing of the detector, which affects the detected signal at wavelengths beyond 7000A, was applied (c.f. Walsh et al. 2003). Figure 6 shows a mosaic of the ten G800L subarray observations of G191B2B, where the sub-arrays have been inserted at their correct positions. The first order spectrum is immediately above the labels in this figure. The second and third orders are to the right of the first order, while the zeroth and negative orders are to the left of the labels.Taking the position of the direct image from the companion direct image and using the flat-field cube described in Section 4, the first order spectra were wavelength calibrated and extracted in counts per second using aXe. A wide extraction window (50 pixels, 2.5arcsec) was used to ensure all the flux was collected.

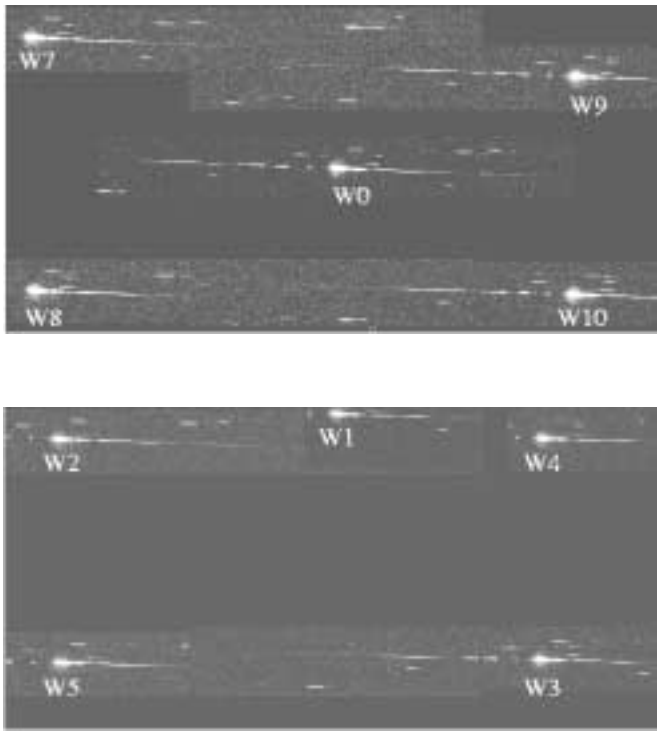

Figure 6: Mosiac image of the ten WFC sub-array observations of G191B2B taken with the G800L grism is shown. CHIP1 is upper; CHIP2 lower.

If the ten extracted spectra are plotted together they do not match perfectly and there are differences in the vertical height in electrons per second as shown in Figure 7 for CHIP1 for example. The feature at 6560A is the H-alpha absorption line in the stellar spectrum; it

provides a good check of the wavelength calibration accuracy. The peak-to-peak range at the maximum count rate of the spectra is 32% of the mean. Since the specification for flux calibration accuracy of ACS spectra is better than 5% (absolute) over the whole field and wavelength range, then clearly flat-fielding is required to meet this goal. **The primary aim of flat-fielding for slitless spectroscopy should be to correct for pixel-by-pixel and field dependent throughput so that by application of a single sensitivity curve, extracted spectra can be converted to absolute flux units, independent of position.** The observations of G191B2B at ten positions over the field these can be used to determine an empirical correction to the flat-field to ensure that the absolute flux calibration is field independent. This empirical correction contains components related to the geometric distortion, which is corrected in the wavelength direction by the spatially dependent dispersion solution, and by any vignetting of the G800L grism itself.

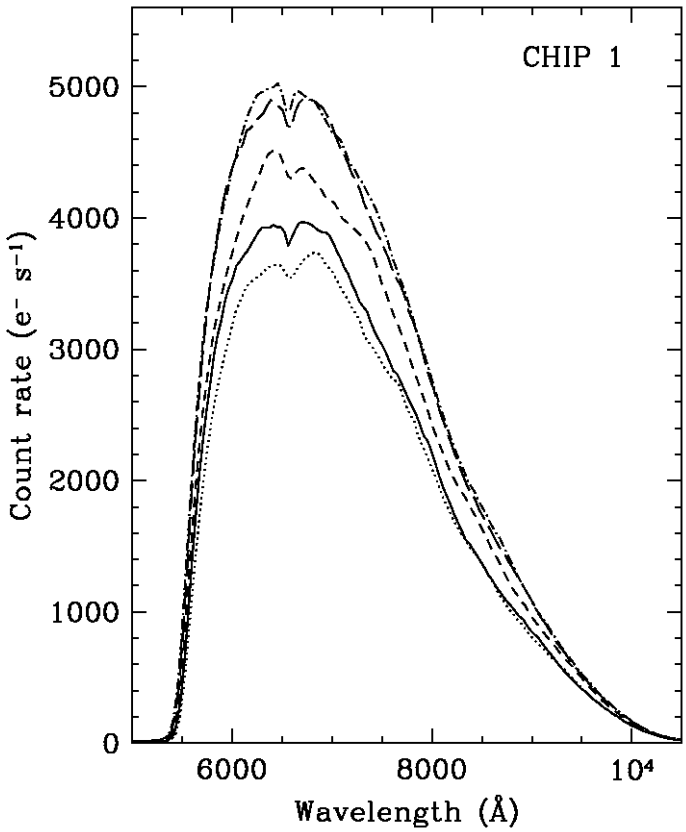

Figure 7: Extracted spectra of G191B2B in units of e/s v. wavelength at five positions over WFC CHIP1 are shown, where no corrected flat-field was applied in the extraction process (see text).

5.2 HRC

The white dwarf GD153 was observed during the ACS SMOV at five positions over the field (proposal 9029). For these observations the full HRC field was employed. However only three of the 1st order spectra are fully contained on the detector and were available for analysis of the sensitivity and flat-field correction. Table 2 contains brief details of the observations. The pointing position refers to the position of the star on the direct image. The HRC raw data were pipeline calibrated and the _FLT files were used for analysis.

Image	Pointing (X,Y pix)	Date	Filters	Exp.(s)
j8ca07g6q	172,572	2002-04-30	F775W	6
j8ca07g7q			G800L	180
j8ca07gcq	732,578	2002-04-30	F775W	6
j8ca07gdq			G800L	180
j8ca07geq	540,196	2002-04-30	F775W	6
j8ca07gfq			G800L	180
j8ca07ggq	172,572	2002-04-30	F775W	6
j8ca07ghq			G800L	180
j8ca08qeq	732,576	2002-04-30	F625W	3
j8ca08qfq			G800L	180
j8ca08qgq	540,196	2002-04-30	F625W	3
j8ca08qhq			G800L	180

Table 2. Log of the observations of GD153 with the ACS HRC in programme 9029

6. Deriving the absolute sensitivity

The sensitivity for the ACS grism modes is derived by extracting the order spectrum of a spectrophotometric standard star in electrons/s, wavelength calibrating it and ratioing it by the tabulated flux. G191B2B and GD153 are two of the HST spectrophotometric standards and have excellent flux data from the UV to the near-IR (Bohlin 2000). aXe requires that the sensitivity curve is in units of $e^- s^{-1}$ per Angstrom per unit flux (ergs $cm^{-2} s^{-1} A^{-1}$). By extracting each order and wavelength calibrating (using the fits in Pasquali et al. 2003a), sensitivity calibrations for orders 1st, 2nd, 3rd and -1st, -2nd can be established for the WFC. An approximate wavelength calibration was established for the zeroth order, based only on the width of the spectrum, since the dispersion is very low (650A/pixel), enabling sensitivity derivation for this order also. For the HRC the wavelength calibration detailed by Pasquali et al. (2003b) was applied and sensitivity calibrations for orders 1, 2, 0 and -1 were determined.

Once the flat-field correction is done accurately then the derivation of the sensitivity should be independent of the position of the observed spectrum on the detector. In order

to reach this condition, a reference position was chosen and the responses elsewehere on the detector were normalised to the flux from the spectrum at the reference position. For the WFC, it was decided to choose CHIP1 position W0 since it is well placed, suffers no losses of signal at the edges and the dispersion solution does not change rapidly with position as in the corners of the field. For the HRC, the most central position (732,578 in Table 2) was chosen.

7. Improving the flat-field cube

7.1 WFC

Using the flat-field derived as described in Section 4 and extracting with aXe the G191B2B first order spectrum at position W0, provided the WFC sensitivity curve shown in Figure 8. The errors arise from the propagated errors on the extracted spectrum based on the count statistics and read-out noise. Adopting this sensitivity calibration, then fluxes for the other extracted spectra at different detector positions can be derived and compared. The rms on the fit is 2.11×10^{-14} ergs cm^{-2} s^{-1} A^{-1} per pixel over the range 5800 to 9000A, a range which is well covered by the wavelength extent of the in-orbit flat-fields. As a fraction of the mean signal over this range, the rms is 5.4%

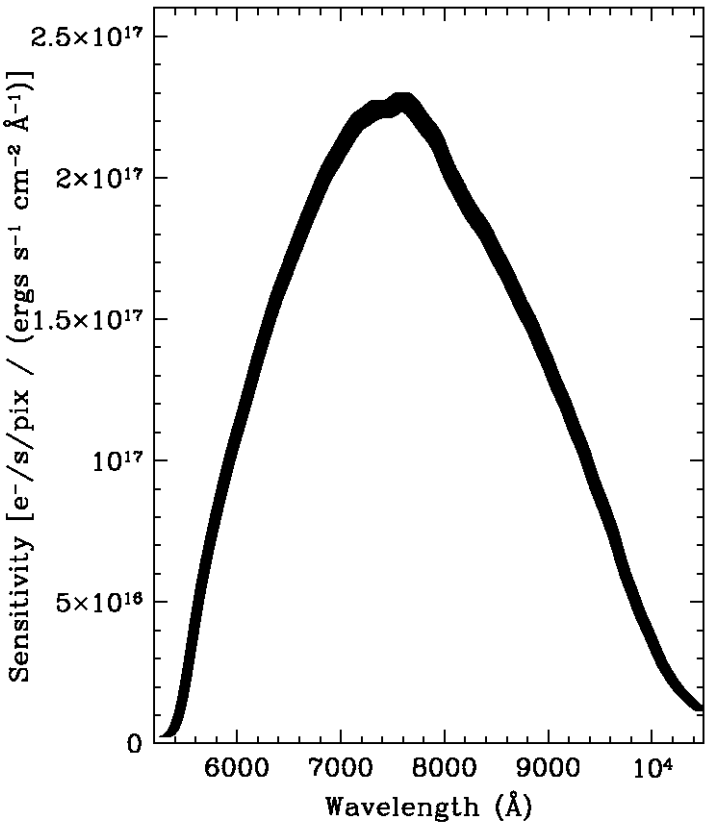

Figure 8: The derived sensitivity file in units of electrons per second per pixel for the WFC based on G191B2B at position W0 of CHIP1. The line is broadened by the error bars.

A scaling factor per spectrum can be derived to ensure that the ten extracted flux calibrated spectra agree better than in Figure 9. By fitting the scaling factors as a function of detector position, a correction image can be derived. A linear slope term was fitted to the flux in each spectrum as a function of X and Y position for each CHIP separately, normalising to the flux of G191B2B at position W0. The slope terms were small - around 10^{-5} per pixel. The correction image for each chip increases from top left to bottom right. This trend can be directly compared to the effect of WFC pixel effective area shown in Fig.6b of Mack et al. 2002. This is explained by the fact that the L filter flats correct for surface intensity, but on account of the geometric distortion, object photometry is not conserved across the field. Since the slitless spectra were not geometrically corrected in the cross-dispersion direction, then the effect of the varying pixel area shows up in this correction image derived from point source photometry. The flat-field correction image was applied to the zeroth order term of the 3rd order polynomial fit to the flat-field with wavelength. Thus the spatial change in the sensitivity resulting from the pixel area correction was put directly into the flat-field, allowing use of a single sensitivity.

Re-extracting the ten spectra, reduced using this modified flat-field and the single sensitivity, produced good agreement, as is evident from Figure 10. The rms on the mean of the ten spectra is 9.7x10-15 ergs cm^{-2} s^{-1} A^{-1} per pixel over the range 5800 to 9000A; this rms is 2.4% of the mean flux over that range. A delta improvement on this adopted sensitivity was made by comparing the mean flux spectrum from all ten positions with the standard star spectrum. The correction is <3% at wavelengths below 9500A but increases at longer wavelengths where the sensitivity declines steeply. Then the new rms, resulting from application of this corrected sensitivity, on the match of the mean of the ten flux-calibrated spectra with the standard star flux is 5.1 $x10^{-15}$ ergs cm^{-2} s^{-1} A^{-1} per pixel over the range 5800 to 9000A; this rms is only 1.3% of the mean flux over that range. This finally adopted sensitivity curve is shown in Figure 8, but in units of electons per pixel per second (using the mean pixel scale for the spectrum at position W0) for more direct comparison with STIS, for example.

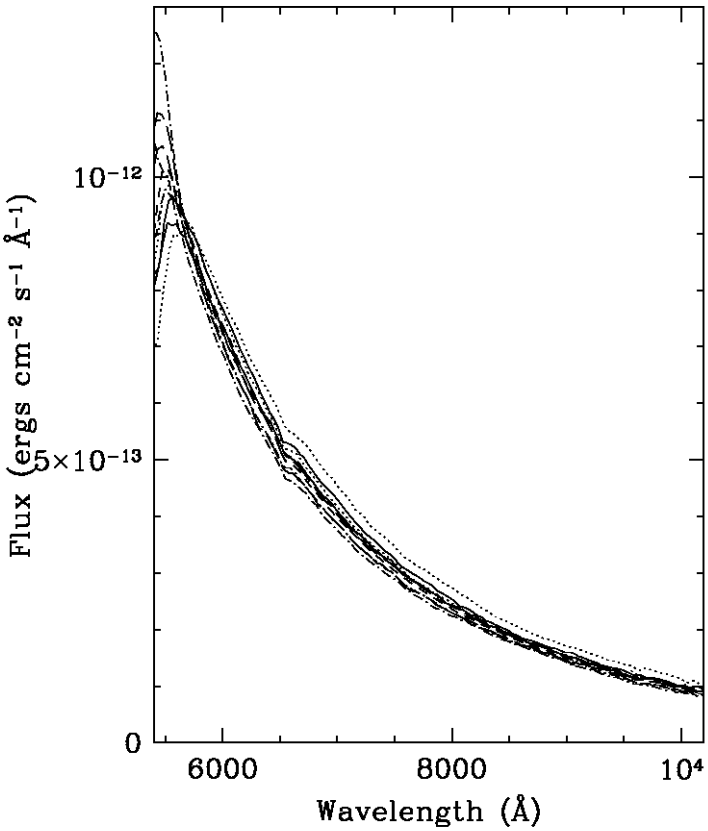

Figure 9: The flux calibrated spectra of G191B2B at the ten positions over the WFC field are shown; the flat-field is from the 3rd order polynomial fit referred to in Section 7.

Of particular interest is the spectral region above 9000A where Lyman-alpha emission and Lyman-break galaxies can be detected at redshifts above 6.4. For the flat-fielding this is a particularly difficult region, since the longest wavelength of the in-orbit flats is 9445A

(F850LP) and the response of the ACS CCD's is falling rapidly. Comparing the mean spectrum of the ten G191B2B flux calibrated observations in the wavelength range 9400-10400A with the standard star flux, shows an rms of 5.2×10^{-15} ergs cm^{-2} s^{-1} A^{-1} per pixel, which is 4.8% of the mean value over this range. The mean flux agrees within 2% of that of the standard star to 10300A but, not surprisingly, deviations to 10% at 10500A are found. There is second order overlap at these wavelengths which has not been decomposed from the first order spectrum, so the sensitivity derived for this blue star would not be reliable for very red objects for example. At wavelengths below about 5800A there is rather a strong disparity between the ten spectra in Figure 9. This is attributable to the very steep drop in the G800L sensitivity. Small errors in the wavelength solution or changes in the PSF will cause large fluctuations in the calibrated flux over this wavelength range.

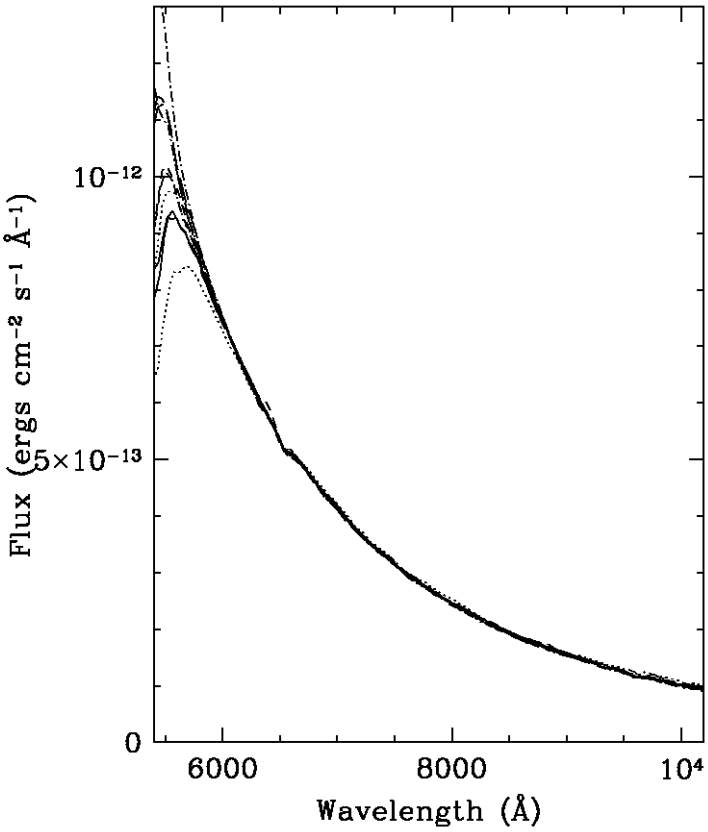

Figure 10: The ten flux calibrated spectra of G191B2B are shown for comparison with Figure 9. Here the modified flat-field, described in Section 7, has been applied.

7.2 HRC

An identical procedure was followed for the HRC. Extracting the spectra of GD153 at the three positions (see Table 2) and comparing them showed no significant differences. It was not therefore justified in modifying the flat-field derived from the least squares fit to the in-orbit flats.The three spectra showed an rms on the mean of 1.1 x 10^{-14} ergs cm^{-2} s^{-1} A^{-1}, per pixel, equivalant to 1.0% of the mean flux over the range 6000-9000A.

8. Interplay of ACS geometric distortion on slitless spectra

There are several reasons why the flat-field derived from the in-orbit flats should not be directly applicable to flat-fielding of the G800L slitless grism spectra. First, it is likely that the large scale flat (L-flat) characteristic of the G800L grism is somewhat different from that of the broad filter flats used to generate the flat-field data cube. Second, the filter L flat-fields produce a flat image for a flat direct image of the sky, but the effective pixel size varies significantly from one corner of the detector to another. In order to provide correct surface and object photometry for slitless spectral data, it is necessary to apply a correction which is related to the geometric distortion. The ACS geometric distortion is partly altered during the aXe extraction process because aXe uses a calibrated field dependence of the dispersion properties of the G800L grism (Pasquali et al. 2002a for the WFC and Pasquali et al. 2003b for the HRC) which already takes into account the effect of the distortion on the dispersion. The extra correction to the in-orbit LP flat-field cube, which was determined from the analysis of the standard star fluxes (Section 7), is in the same sense as the geometric distortion - viz. largest correction is at the top left of the chips, the lowest correction at the lower right. The geometric distortion gives rise to a corner-to-corner change in pixel area of about 14% over each chip (slightly higher for CHIP1 than CHIP2, see http://www.stsci.edu/hst/acs/analysis/PAMS), whilst the flat-field correction image derived from the standard star spectra amounts to 17 and 14% across CHIP 1 and 2 respectively. Part of this difference between the pixel area correction and the correction term for spectra could arise from a component related to the spatial transmission of the grism. However given the low order fits to the few points per chip used in deriving the correction images, no firm conclusions on the spatial transmission of the grism can be derived.
In earlier versions of aXe, to version 1.3, no correction for the changing pixel size in the cross-dispersion direction, which arises from the geometric distortion, was applied to the flat-field output stamp 2D spectra. This was changed in aXe1.4 where individual spectra are now drizzled onto a rectified wavelength cross-dispersion grid, specified in A and arcsec respectively (thus implementing a pixel length correction in the cross-dispersion direction). The sensitivity calibration applies to extracted spectra with and without drizzling in the cross-dispersion axis. The new approach simplifies the combination of dithered spectra and ensures that the cross-dispersion profile matches for spectra of the

same target taken at different positions on the detector (most relevant for extended objects).

9. Provision of the calibration files

Table 3 lists the flat-fields and sensitivity files which have resulted from this work. They are available on the aXe web page. All are applicable to ACS slitless spectra taken during the in-orbit life of the instrument and are available for download from:
http://www.stecf.org/instruments/acs/calib/Cycle11/WFC/
for the WFC and:
http://www.stecf.org/instruments/acs/calib/Cycle11/HRC/
for the HRC. Since no spectra of the standard stars were available for the HRC 3rd and minus 2nd order sensitivities, they were created by scaling the respective WFC sensitivites by the ratio of the HRC 1st order to the WFC 1st order response.

Channel	Flatfield	Spectral order	Sensitivity file
WFC	WFC.flat.cube.CH1.2.fits	1	ACS.WFC.1st.sens.6.fits
	WFC.flatcube.CH2.2.fits	2	ACS.WFC.2nd.sens.5.fits
		3	ACS.WFC.3rd.sens.5.fits
		0	ACS.WFC.0th.sens.1.fits
		-1	ACS.WFC.-1st.sens.1.fits
		-2	ACS.WFC.-2nd.sens.1.fits
		-3	ACS.WFC.-3rd.sens.1.fits
HRC	HRC.flatcube.2.fits	1	ACS.HRC.1st.sens.2.fits
		2	ACS.HRC.2nd.sens.2.fits
		3	ACS.HRC.3rd.sens.1.fits
		0	ACS.HRC.0th.sens.1.fits
		-1	ACS.HRC.-1st.sens.1.fits
		-2	ACS.HRC.-2nd.sens.1.fits

Table 3. Listing of ACS WFC and HRC flat-field and sensitivity files for use in spectral extraction

11. Conclusions

The construction of the flat-field cube for correcting extracted ACS slitless spectra for the wavelength dependence of the large scale and pixel response has been described. The flat-field cubes are 3rd order polynomial fits to the wavelength dependence determined from the in-orbit flats. The ground monochromatic flats were found not to be suitable for flat-field cube creation on account of illumination effects in the measurement process. A correction image was empirically determined so that wavelength and flux calibrated spectra

of a WD standard star, observed at different places in the field, agreed in absolute flux. On the basis of the mean of spectrum of G191B2B formed from observations at ten different positions over the WFC, the rms scatter of a single spectrum appears to be within 1% over the range 6000 to 9300A, climbing to 4% at 5500A and 6% at 10300A.

Acknowledgements

We would like to thank Wolfram Freudling for valuable comments on the ISR and Richard Hook for help in clarifying how drizzle affects slitless spectra.

References

Bohlin, R., 2000. AJ, 120, 437
Bohlin, R., Hartig, G., 2002. Instrument Science Report ACS 2002-004
Fruchter, A., Hook, R. N., 2002. PASP, 114, 144.
Mack, J., Bohlin, R., Gilliland, R., van der Marel, R., Blakeslee, J., de Marchi, G., 2002. Instrument Science Report ACS 2002-008.
Pasquali, A., Pirzkal, N., Walsh, J. R., 2003a. Instrument Science Report ACS 2003-01
Pasquali, A., Pirzkal, N., Walsh, J. R., 2003b. Instrument Science Report ACS 2003-07
Pavlovsky, C., et al., 2004. ACS Instrument Handbook Version 5.0, STScI
Pirzkal N., Pasquali A., Demleitner M., 2001, ST-ECF Newsletter 29, p. 5
van der Marel, R., 2003, ACS Instrument Science Report ACS 2003-10
Walsh, J. R., Freudling, W., Pirzkal, N., Pasquali, A., 2003. Instrument Science Report ACS 2003-012